ELSEVIER

Thin Solid Films 412 (2002) 129–138

thin solid films

www.elsevier.com/locate/tsf

MBE growth and characterization of Hg based compounds and heterostructures

C.R. Becker*, X.C. Zhang, K. Ortner, J. Schmidt, A. Pfeuffer-Jeschke, V. Latussek, Y.S. Gui, V. Daumer, J. Liu, H. Buhmann, G. Landwehr, L.W. Molenkamp

Physikalisches Institut der Universität Würzburg, Am Hubland, 97074 Wurzburg, Germany

Abstract

The MBE growth of $Hg_{1-x}Cd_xTe$ alloys and type III HgTe/$Hg_{1-x}Cd_xTe$ heterostructures has been discussed, including similarities and differences between the (0 0 1) and (1 1 2)B orientations. Furthermore the MBE growth of HgTe based quantum wells (QWs) with the incorporation of Mn are additional topics. An investigation of the optical properties of type III superlattices with a normal band structure has lead to information about band structure of these heterostructures as well as information about the interface and the semimetallic QW. For example, by means of the full 8×8 Kane Hamiltonian in the envelope function approximation, it has been demonstrated that the energy separation between the H1–E1 and L1–E1 intersubband transition energies is primarily determined by the valence band offset, Λ, between HgTe and CdTe. This has led to unambiguous values for the offset and its temperature dependence, i.e. $\Lambda(T)=570\pm60$ meV and $d\Lambda/dT=-0.40\pm0.04$T meV/K. Furthermore the energy gap of HgTe at room temperature has also been determined. Magneto-transport measurements of n-type QWs show very pronounced Shubnikov-de Haas (SdH) oscillations and well developed quantum Hall plateaus for temperatures up to approximately 60 K. A large Rashba spin–orbit splitting of the first conduction subband, H1, has been observed in HgTe/$Hg_{1-x}Cd_xTe$ QWs with an inverted band structure. Self-consistent Hartree calculations of the band structure based on the above model allows us to quantitatively describe the experimental results and demonstrates that the heavy hole nature of the H1 subband greatly influences the spatial distribution of electrons in the QW and thus enhances the Rashba spin splitting, i.e. $\Delta E_{H1}=\beta k_{\|}^3$. Furthermore, the presence of two periodic SdH oscillations in p-type QWs with an inverted band structure has been observed and is the first direct evidence that these heterostructures are indirect semiconductors. The influence of Mn in the upper barrier on the 2D electrons in the well has been investigated as a function of their separation. With spacer thicknesses of 10 and 15 nm, no appreciable change is observed, however, a reduction of the spacer thickness to 5 nm results in an increase in the maximum population difference between the two Rashba spin split H1 subbands by a factor of approximately two.

Keywords: Molecular beam epitaxy growth; HgTe; $Hg_{1-x}Cd_xTe$; Superlattices; Quantum wells; Valence band offset; Band structure; Rashba spin splitting; Indirect band gap

1. Introduction

The $Hg_{1-x}Cd_xTe$ alloy has been one of the most commercially exploited alloys in recent decades. Both bulk samples and epitaxial layers over the entire composition range can be produced. Due to applications requiring increasingly complex heterostructures [1], molecular beam epitaxy (MBE) is now one of the more important growth techniques. The MBE growth and the dependence of the composition and surface structure on crystal orientation will be discussed. The topics include surface structure, incorporation of Hg and Cd, n and p type doping, modulation doping of both n and p type quantum wells (QWs), etc.

The band structure and hence the optical and electrical properties of type III heterostructures are largely determined by that of the QW. For example the band gap of HgTe and its temperature dependence directly influences the temperature dependence of the superlattice (SL) subbands and thus the temperature dependence of the intersubband transition energies [2]. The magnitude of the negative band gap of HgTe at room temperature is subject to large experimental uncertainties due to difficulties in the conventional magneto-optical method at temperatures above 100 K [3]. Another such property is the deformation potential of HgTe relative to that of CdTe which has only recently been experimentally

*Corresponding author.
E-mail address: becker@physik.uni-wuerzburg.de (C.R. Becker).

0040-6090/02/$ - see front matter
PII: S0040-6090(02)00324-3

determined by means of an optical absorption investigation of $HgTe/Hg_{0.32}Cd_{0.68}Te$ SLs under hydrostatic pressure [4]. Furthermore, it has been shown that the valence band offset is to a good approximation primarily responsible for the energy difference between the first heavy hole, H1, and the first light hole, L1, subband of a $HgTe/Hg_{1-x}Cd_xTe$ SL with normal band structure [2]. This energy difference is nearly independent of other SL parameters, and consequently leads to a precise determination of the valence band offset, Λ, between HgTe and CdTe.

The band structure and consequently the optical properties depend on the band structure of the QWs and barriers, i.e. HgTe and $Hg_{1-x}Cd_xTe$, their widths, and the potential energy differences between these two components. The latter depends in turn on their composition, the valence band offset as well as the shape and width of the Cd concentration profile across the interfaces. A profile described by an error function similar to an experimental profile according to Kim et al. [5] is assumed and leads to a consistent description of the experimental results. Finally, the width of this interface, d_i, has been shown to be a convenient variable for the study of interdiffusion in these SLs [6].

If the HgTe layer is less than 6 nm thick then the heterostructure is a normal semiconductor, however, if the thickness is greater than 6 nm then the band structure is inverted, i.e. the Γ_6 and Γ_8 bands exchange places and the energy gap is negative. Magneto-transport experiments have been conducted on both n and p type modulation doped $HgTe/Hg_{1-x}Cd_xTe$ QWs with an inverted band structure. An analysis of Shubnikov-de Haas (SdH) oscillations in gate controlled n type QWs reveals a large Rashba spin–orbit splitting [7,8]. This is due to the heavy hole character of the first conduction subband. In a p-type QW two periodic SdH oscillations are observed which are caused by the indirect band structure [9].

2. Experimental details

The epitaxial alloys and heterostructures were grown in a Riber 2300 MBE system as has been described elsewhere [2,10]. After the growth of a thin CdTe buffer layer, the alloys and heterostructures were grown on (0 0 1) and (1 1 2)B oriented $Cd_{0.96}Zn_{0.04}Te$ substrates at 180 °C. The (0 0 1) QWs were modulation doped symmetrically, on both sides of the QW, and asymmetrically, on one side only, with either iodine or arsenic for n and p type structures, respectively. The $Hg_{0.3}Cd_{0.7}Te$ barriers are comprised of a 50 Å thick spacer and a 90 Å thick doped layer.

Asymmetric $HgTe/Hg_{0.3}Cd_{0.7}Te$(0 0 1) modulation doped n type QWs, were grown with Mn in the upper barrier. Mn is separated from the HgTe layer by means of a $Hg_{0.3}Cd_{0.7}Te$ spacer, which was varied between 5 and 15 nm. Then a $Hg_{0.3}Cd_{0.7}Te$ cap was grown, thereby maintaining the same total thickness of all layers above the HgTe layer, i.e. 34 nm.

The composition of the barrier material [11] has been determined by means of transmission measurements on thick test layers of $Hg_{1-x}Cd_xTe$ grown under identical conditions. SL periods and HgTe(0 0 1) layer widths have been determined via a dynamic simulation of the (0 0 2) and (0 0 4) Bragg reflections measured in a six crystal X-ray diffractometer [2]. A simulation of (1 1 2)B oriented heterostructures is more complicated and the results less accurate [12,13].

After growth of the QWs, standard Hall bars were fabricated by means of a wet chemical etch, then a 200 nm thick Al_2O_3 film, which serves as an insulating layer, was deposited by electron beam evaporation. Finally Al was evaporated to form a gate electrode.

Optical transmission measurements were carried out in the middle and near infrared with a Fourier transform spectrometer, Bruker IFS88. A $LiTaO_3$ detector was usually employed rather than a liquid nitrogen cooled detector e.g. $Hg_{1-x}Cd_xTe$, because of its better linearity. The aperture was kept as small as possible for the same reason, i.e. a diameter of 2–3 mm. The absorption coefficient, α, was determined by fitting the experimental transmission spectra to a theoretical description of the multi-layer system using standard matrix procedures [14].

3. Theoretical details

A large number of **k·p** band structure calculations using the envelope function approximation for the $HgTe/Hg_{1-x}Cd_xTe$ SL have been published during the last decade [15–18]. A brief review of these and other investigations pertinent to the results presented here can be found in Ref. [2].

The bands of both bulk HgTe and CdTe are described by Kane's four-band model (8×8 **k·p**) including second-order remote band contributions. The envelope function method has been used to calculate the band structure of the HgTe/CdTe SL. The results of the axial approximation are not exact, however, they give a good approximation, within 1 or 2 meV, for the subband energies at $k_{\|}=0$ as well as for an average of the subband dispersion over all $k_{\|}$ directions. Consequently all absorption coefficient calculations and most intersubband transition energy calculations were carried out using an adapted Hamiltonian in the axial approximation, in order to reduce the calculation time.

The effects of strain due to lattice mismatch were also taken into consideration. The lattice mismatch between HgTe and its environment is less than 0.1% which results in a shift in intersubband transition energies of less than 3 meV and can therefore be neglected. In contrast to the [0 0 1] direction [17], the strain tensor

for the [1 1 2] direction has a shear strain component. This results in a piezoelectric field in the growth direction [19]. We have calculated the strain for a free standing, strained (1 1 2)B SL and a fully strained (1 1 2)B SL on a $Cd_{0.96}Zn_{0.04}Te$ substrate. From these results the piezoelectric field has been calculated to be less than 5 mV/100 Å whose influence on intersubband transition energies is less than 1 meV and can therefore be neglected in the calculations.

A revised set of values for the band parameters (Δ= 1.0 eV, $\gamma_1=4.1$, $\gamma_2=0.5$, $\gamma_3=1.3$, $F=0$ and $E_p=18.8$ eV) deduced from measurements on bulk HgTe and $Hg_{1-x}Cd_xTe$ by Weiler [20] were employed which nevertheless reproduce the same bulk band structure:

$$m^*_{hh}(1\,1\,2)=\left(\gamma_1-2\gamma_2-\frac{3}{2}(\gamma_3-\gamma_2)\right)^{-1}m_0 =0.53m_0 \quad (1)$$

and

$$m^*_{hh}(0\,0\,1)=(\gamma_1-2\gamma_2)^{-1}m_0=0.32 \quad \text{at 5 K.} \quad (2)$$

The energy gaps of HgTe and $Hg_{1-x}Cd_xTe$ were taken from the empirical $E_g(x, T)$ relationship according to Laurenti et al. [11] with the exception of HgTe at temperatures greater than 5 K as discussed below. The valence band offset between HgTe and $Hg_{1-x}Cd_xTe$ is employed as an adjustable variable and is assumed to vary linearly with x for $Hg_{1-x}Cd_xTe$, i.e. $x\Lambda$ [21]. An interface width, d_t, which results during growth or from interdiffusion of the two types of layers was integrated into the theory. The concentration profile across the interface is described by an error function similar to an experimental profile according to Kim et al. [5].

Self-consistent Hartree calculations of modulation doped HgTe/$Hg_{1-x}Cd_xTe$ QWs have been carried out using Kane's four-band model (8×8 **k·p**) described above in order to quantitatively describe the observed Rashba spin–orbit splitting, see Ref. [8] for details.

4. Results and discussion

4.1. Growth and characterization of $Hg_{1-x}Cd_xTe$

The growth of undoped $Hg_{0.80}Cd_{0.20}Te$(1 1 2)B has been investigated with regard to the mobility μ and the surface structure [22]. The mobility has a maximum value of approximately 3×10^5 cm^2 V^{-1} s^{-1} for a Hg/Te flux ratio of between 150 and 180. In contrast the void density has a maximum value of 6×10^5 cm^{-2} at low ratios and falls rapidly to a nearly constant value of 2×10^3 cm^{-2} for ratios $\geqslant$200. At a ratio of 180 the void density is approximately 4×10^3 cm^{-2}. In order to obtain maximum mobilities, a Hg/Te flux ratio of 180 was employed for the n-type layers in this investigation. Hence these samples have slightly higher void densities than the minimum values.

The optimum Hg/Te flux ratio for the (1 1 2)B orientation is about half of the optimum value for $Hg_{0.80}Cd_{0.20}Te$(0 0 1) according to He et al. [23]. The latter value was chosen with regard to mobility and density of hillocks. Obviously the incorporation of Hg is more efficient in the (1 1 2)B alloys. This is also the case for Cd; the Cd/Te flux ratio necessary to grow an (1 1 2)B alloy with $x=0.20\pm0.01$ at 180 °C is approximately 20–30% smaller than the ratio needed for the same composition in the (0 0 1) orientation [10]; and a (1 1 2)B alloy grown with only the CdTe and Hg sources results in $x=0.95\pm0.02$, but a (0 0 1) alloy grown under the same conditions has a composition given by $x=0.68\pm0.02$ [2].

The n and p type doping of $Hg_{1-x}Cd_xTe$ has been investigated using iodine in the form of CdI_2, and either arsenic as Cd_3As_2 or plasma activated nitrogen, respectively. n Type doping has been successful for the (0 0 1) and (1 1 2)B orientations [10,22] over the entire composition range with the exception of large Cd concentrations in the (1 1 2)B orientation. Producing p type alloys is more difficult and to our knowledge in situ doping has never been consistently successful. There is one exception; CdTe can be p type doped with plasma activated nitrogen up to concentrations of approximately 10^{18} cm^{-3}, however, at high charge carrier concentrations the crystalline quality is adversely effected. Normally p type doping of the alloy with As requires an ex situ anneal in Hg vapor at high temperatures. Nevertheless p type conductivity has been achieved in HgTe QWs by means of in situ doping and activation of Cd_3As_2 in a CdTe layer [24].

A low resolution atomic force microscope (AFM) image of an $Hg_{0.80}Cd_{0.20}Te$(1 1 2)B epitaxial layer is shown in Fig. 1. Long parallel ridges and trenches are observed whose height difference is approximately 30 Å. These ridges and trenches are parallel to the edges of the sample, i.e. the {1 1 0} surface. The (1 1 2)B surface can be thought of as an (1 1 1)B surface with a high ledge density [25]. If the height of the individual steps is the distance between nearest neighbors, i.e. between cation and anion, then the distance between steps is 11.2 Å. Experimentally, a pattern in the reflection of high energy electron diffraction is observed whose period in real space is 11.1 ± 0.3 Å, which is in very good agreement with the above step width. These microscopic edges are parallel to the [1 1 0] direction and consequently parallel to the ridges and trenches shown in Fig. 1. Apparently preferential growth along these ledges result in these trenches and ridges.

The $Hg_{0.80}Cd_{0.20}Te$(0 0 1) surface [22], is radically different. Nearly elliptically shaped mounds with a height of approximately 300 Å are observed which are similar to the mounds observed on the HgTe(0 0 1)

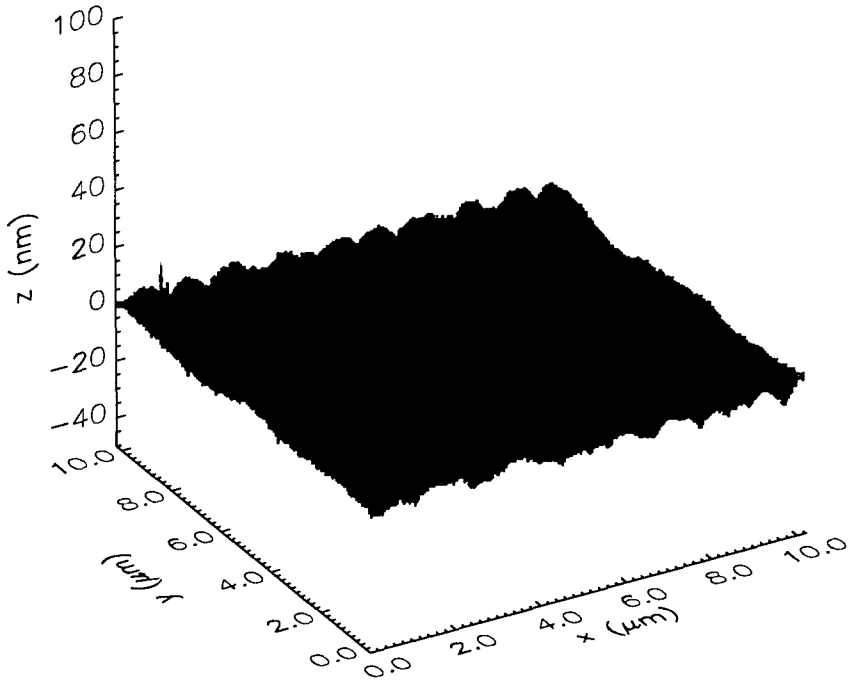

Fig. 1. A low resolution AFM image of a $Hg_{0.80}Cd_{0.20}Te(1\ 1\ 2)B$ epitaxial layer.

surface by Oehling et al. [26] with a scanning tunnel microscope. The latter mounds consist of a series of terraces whose height is that of one monolayer, i.e. 3.2 ± 0.3 Å, and width is approximately 500 Å. A high resolution AFM image of an $Hg_{0.80}Cd_{0.20}Te(1\ 1\ 2)B$ surface demonstrates that these long ridges also consist of terraces whose height difference is one monolayer and average width is approximately 180 Å [22].

4.2. Optical absorption; intersubband transitions in SLs

The experimental and theoretical absorption spectra for a (1 1 2)B $HgTe/Hg_{0.05}Cd_{0.95}Te$ SL at 5 K are shown in Fig. 2. Three distinctive steps are observed which we have assigned to the H1–E1, L1–E1 and H2–E2 intersubband transitions. H, L and E are the heavy hole, light hole and electron subbands, respectively. In contrast, Yang et al. [27] attributed the first two steps at lower energies in a similar SL to the H1–E1 and H2–E2 transitions, and the weak shoulder near 240 meV to L1–E1. A correct assignment requires agreement between the calculated transition probabilities and the observed absorption coefficient spectrum as well as between the calculated and experimental frequencies. That this is the case here, is demonstrated in Fig. 2. The relative heights of the three steps are in good agreement with experiment, even though their absolute magnitudes are underestimated due to the neglect of Coulomb interaction between electron and hole [28]. The energies of the H1–E1 and L1–E1 transitions are in good agreement whereas agreement is only fair at higher energies, e.g. for H2–E2, as expected for a perturbation theory. The weak shoulder near 240 meV is due to the H2–E1 transition which is allowed only for $\mathbf{k}>0$. For these reasons and others which will become apparent below, we shall concentrate on the H1–E1 and L1–E1 transitions.

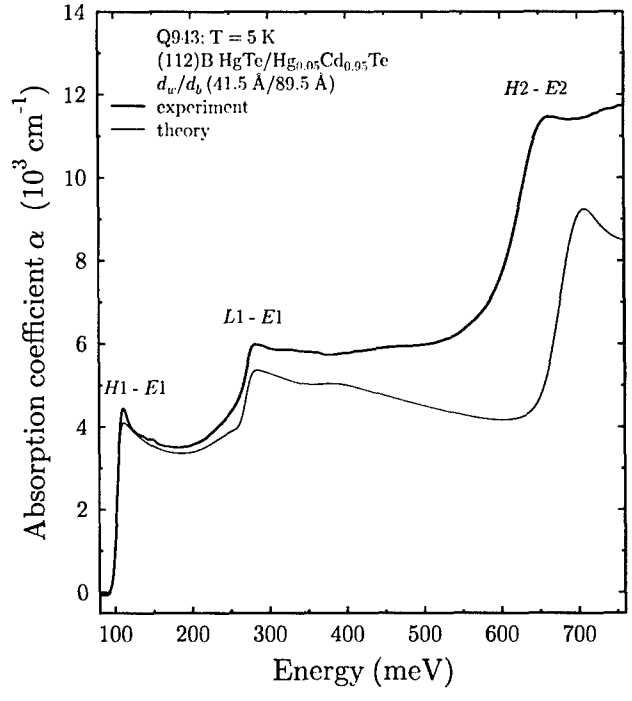

Fig. 2. The experimental and theoretical absorption coefficients of the (1 1 2)B $HgTe/Hg_{0.05}Cd_{0.95}Te$ SL Q943 at 5 K.

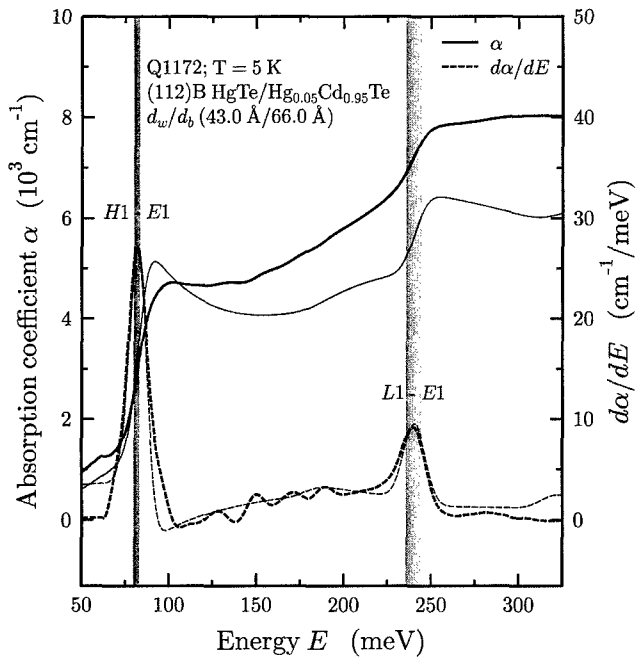

Fig. 3. The experimental (thick line) and theoretical (thin line) absorption coefficients, their first derivatives (thick and thin dashed lines, respectively) for the (1 1 2)B $HgTe/Hg_{0.05}Cd_{0.95}Te$ SL Q1172 at 5 K. The intersubband transition energies are indicated by vertical lines and their dispersion for $\mathbf{q}\|\mathbf{z}$, the miniband width, by the width of these vertical lines

A determination of the experimental intersubband transition energies is not trivial, due largely to a lack of knowledge about the position of a particular band gap relative to the frequency of photoluminescence peaks [27,29,30], or that of the absorption edges [31]. The method employed by Becker et al. [2] is to determine the position of the absorption edge and then its position relative to the intersubband transition energy itself. This can be accomplished by calculating the transition energies as well as the corresponding absorption coefficient. Finally, by fitting the theoretical and experimental absorption coefficients, one can determine the experimental intersubband transition energies relative to their absorption edges.

The absorption edges have been determined by two different methods. In the first method, the absorption edge is defined as the energy at the maximum value of the first derivative of the absorption coefficient. In the second method the absorption edge is determined from the temperature dependence of the transmission according to

$$\frac{\Delta T}{T} = \frac{T_2}{T_1} - 1 \approx d\Delta\alpha \qquad (3)$$

where T and d are the transmission and sample thickness, respectively. Hence a good approximation of $\Delta\alpha$ can be obtained merely from a ratio of transmission spectra at slightly different temperatures [2] without the complications and uncertainties in calculating the absorption spectrum of the SL in a multi-layer structure [14]. The absorption edges according to both of these methods coincide with the H1–E1 and L1–E1 intersubband transition energies to within ± 2 meV for all investigated SLs with one exception in which a systematic discrepency of 4 meV for L1–E1 is observed [2].

Good agreement between experimental and theoretical values of the absorption edges, i.e. $d\alpha/dE$, is demonstrated for a (1 1 2)B orientated SL in Fig. 3. The full width at half maximum, FWHM, of $d\alpha/dE$ for the H1–E1 and L1–E1 intersubband transitions is approximately 13 and 16 meV, respectively, and thus sufficiently narrow to allow a determination of these energies with a precision of ± 2 meV or better. The absorption edges for Q943 shown in Fig. 2 are even sharper with corresponding FWHMs of 8.5 and 12 meV.

The H1–E1 and L1–E1 intersubband transition energies at 5 K for all of the investigated (1 1 2)B SLs are plotted vs. QW width, d_w, in Fig. 4. Also shown is the energy difference between these two intersubband transitions, i.e. $E_{H1}-E_{L1}=E_{L1-E1}-E_{H1-E1}$. The strong inverse dependence of both transitions on d_w is obvious, whereas $E_{H1}-E_{L1}$ is nearly independent of d_w. The latter energy difference depends nearly linearly on the valence band offset, Λ. Hence a determination of Λ is possible which is not influenced by uncertainties in d_w. The three sets of lines in Fig. 4 are theoretical results for a series

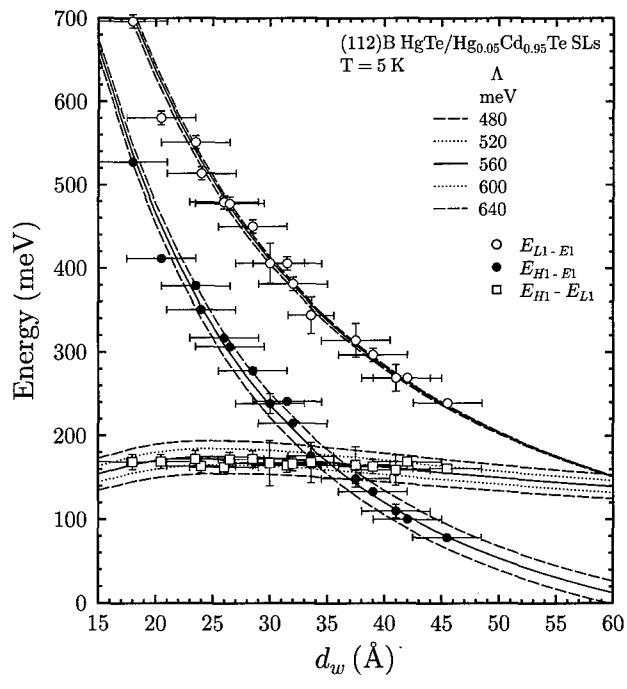

Fig. 4. The experimental values for E_{H1-E1} (filled circles), E_{L1-E1} (empty circles) and the energy difference, $E_{H1}-E_{L1}$ (empty squares), for all (1 1 2)B SLs together with theoretical results at 5 K (lines) are plotted vs. d_w. Calculated results using $d_i=24$ Å for possible values of Λ are shown. d_i is the interface width.

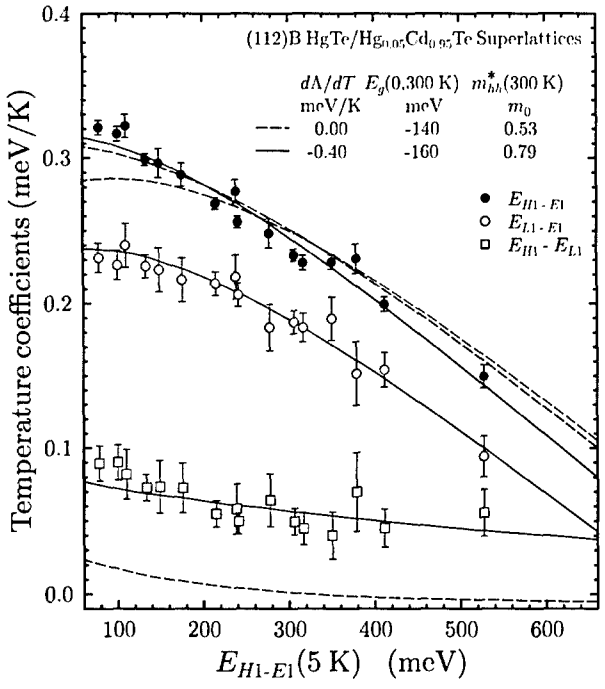

Fig. 5. Linear temperature coefficients for E_{H1-E1} (filled circles), E_{L1-E1} (empty circles) as well as $E_{H1}-E_{L1}$ (empty squares) are plotted vs. E_{H1-E1} at 5 K for all (1 1 2)B SLs. Calculated results for $d\Lambda/dT=0.00$ meV/K and E_g(HgTe, 300 K) = −140 meV are reproduced as dashed lines, and the results when $d\Lambda/dT=-0.40$ meV/K, E_g(HgTe, 300 K) = −160 meV and in addition m^*_{hh} is temperature dependent, i.e. $m^*_{hh}=0.79m_0$ at 300 K, as solid lines.

of Λ values. By means of an error analysis involving all relevant bulk and SL parameters together with their uncertainties, the valence band offset between HgTe and CdTe has been determined to be $\Lambda=570\pm60$ meV for both the (0 0 1) and (1 1 2)B orientations [2]. A detailed comparison of this value and literature values can be found in Ref. [2].

Experimental values of $E_{H1}-E_{L1}$ display a significant temperature dependence [2]. Therefore according to the conclusions presented above, Λ is also temperature dependent. Linear temperature coefficients have been calculated for the three pertinent energies using the SL parameters determined below. The calculated results are obviously in excellent agreement with the experimental values according to Ref. [2]. Because the temperature dependence of $E_{H1}-E_{L1}$ is linear within experimental uncertainties, the authors concluded that this is also the case for Λ.

The temperature dependence has been determined using a procedure which relies only on experimentally determined energies and not on d_w or other SL parameters. This is illustrated in Fig. 5 where the temperature coefficients for E_{H1-E1}, E_{L1-E1} and $E_{H1}-E_{L1}$ are plotted vs. E_{H1-E1} (5 K) for the (1 1 2)B SLs. The dashed lines are results of the theory when Λ is assumed to be temperature independent and the energy gap of HgTe at room temperature, E_g(0, 300 K), is taken to be −140 meV [32]. Even though the temperature dependence of the H1–E1 transition can be reproduced, this is clearly not the case for either L1–E1 or the energy separation between these two transitions, $E_{H1}-E_{L1}$. Consequently the results of previous investigations, which are based merely on the H1–E1 transition can be misleading. For example the conclusion of von Truchsess et al. [33] that Λ is temperature independent, is obviously incorrect.

It has been demonstrated that the temperature dependence of the L1–E1 intersubband transition is determined by the temperature dependence of both the HgTe band gap and Λ. A least square fit to the experimental values of L1–E1, shown as a solid line in Fig. 5, results in $E_g(0,\ 300\ K)=-160\pm2$ meV and $d\Lambda/dT=-0.40\pm0.04$ meV/K [2], which are listed in Table 1. This value for E_g(0, 300 K) differs appreciably from literature values of −140 and −120 meV [11,32], which clearly lie outside of the experimental uncertainties in this investigation. However, these two values are not experimental values: they have been determined by extrapolating experimental results for $T<100$ K up to room temperature.

On the basis of X-ray photoemission spectroscopy, and ultra violet spectroscopy (UPS) Sporken et al. [34] concluded that the valence band offset between CdTe and HgTe was independent of temperature between 50 K and room temperature with an uncertainty of ±0.25 meV/K. However the valence band offset was not determined at $\mathbf{k}=0$: their UPS samples were sputtered and they employed the He I and He II emission lines whose energies correspond to a position in the Brillouin zone far removed from $\mathbf{k}=0$ [35].

The results for E_{H1-E1} and $E_{H1}-E_{L1}$ using $d\Lambda/dT=-0.40$ meV/K and $E_g(0, 300)=-160$ meV are in good

Table 1
Experimentally determined values together with their uncertainties for E_g(0, 300 K), Λ_0, Λ(300 K), $d\Lambda/dT$ and m^*_{hh}(300 K), for the (1 1 2)B and (0 0 1) orientations

	E_g(0, 300 K) meV	Λ_0 meV	Λ(300 K) meV	$d\Lambda/dT$ meV/K	m^*_{hh}(5 K)[a] m_0	m^*_{hh}(300 K) m_0
(1 1 2)B	−160±2	572±60	452±60	−0.40±0.04	0.53	0.79±0.04
(0 0 1)	−157±4	566±60	458±60	−0.41±0.10	0.32	0.40±0.11

The valence band offset is given by $\Lambda(T)=\Lambda_0+(d\Lambda/dT)T$.
[a] After Ref. [20].

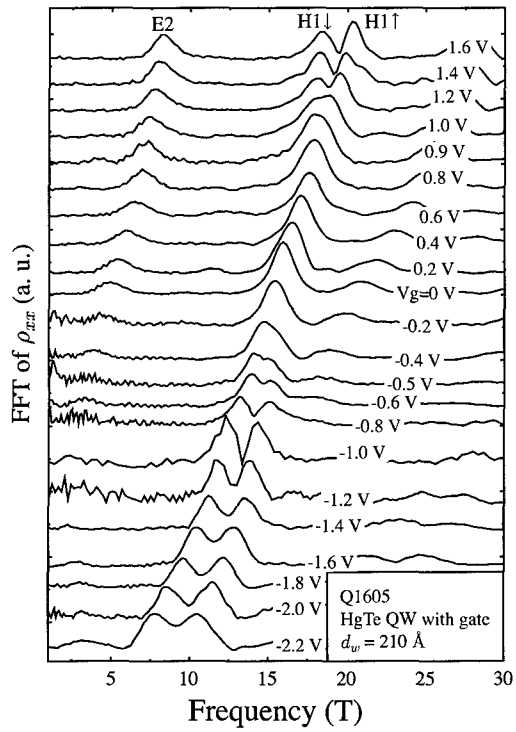

Fig. 6. FFT of SdH oscillations in $\rho_{xx}(B)$ for a n type symmetrically modulation doped HgTe QW (Q1605) measured at 1.6 K and various gate voltages. The up and down arrows represent the two spin states of the H1 subband.

agreement with experiment at lower values of E_{H1-E1} (5 K) as previously reported [36], however, at higher energies this is not the case [2]. Better agreement with experiment over the entire energy range can only be achieved by assuming that the heavy hole effective mass is also temperature dependent. A least square fit to the experimental values of E_{H1-E1}, which is shown as a solid line in Fig. 5 results in $m^*_{hh}(1\,1\,2) = 0.79 \pm 0.04 m_0$ at 300 K [2], see Table 1.

The experimental temperature dependence of E_{L1-E1} and E_{H1-E1}, as well as that of $E_{H1}-E_{L1}$ cannot be explained unless Λ and m^*_{hh} are temperature dependent. Within experimental error the results for the (0 0 1) and the (1 1 2)B orientations are equivalent [2] as can be seen in Table 1, with the exception of the heavy hole effective mass as expected according to Eq. (1) and Eq. (2).

4.3. Magneto-transport; n type modulation doped QWs

As expected from their high electron mobility, all n type, modulation doped QWs show very pronounced SdH oscillations and well developed quantum Hall plateaus [8]. The results of a Fourier transformation of the complex SdH oscillations for the symmetrically modulation doped sample Q1605 with a well width of 21 nm are shown in Fig. 6. At a gate voltage, V_g, of 0.2 V, when the QW potential is nearly symmetric only two frequencies, which correspond to the H1 and E2 subbands, are resolved and no splitting of the H1 subband can be observed. For either more positive or more negative gate voltages, a large splitting of the H1 subband is apparent. Besides the main peaks labelled by E2, H1+ and H1−, peaks due to the sums of the E2 and H1 peaks can be observed. The largest Hall mobility was 6×10^5 cm^2 V^{-1} s^{-1} at a gate voltage of 2.0 V; to our knowledge this is the highest value that has been observed for HgTe QWs.

According to self-consistent band structure calculations the first two conduction subbands are H1 and E2, and the valence band is the H2 subband. This is a consequence of the inverted band structure of QWs with a large well width. No splitting of the H1 and E2 subbands for the symmetric case was predicted and none was observed [8]. However, in the asymmetric case, a small spin splitting of the E2 subband at finite $k_\parallel$ is predicted as well as a substantially larger splitting of the H1 subband. It should be mentioned here that the two spin split branches of the H1 subband cannot be designated as spin-up and spin-down because their eigenstates are not linearly polarized and do not carry a net magnetic moment [37]. The H1 and E2 subbands which are a mixture of states with different symmetries contain an equal contribution of up and down spinor components at finite $k_\parallel$. The degeneracy of the H2 valence subband is also removed and one spin component has a larger maximum at finite $k_\parallel$, i.e. here we are dealing with an indirect semiconductor.

The experimental values and the theoretical calculations of the difference in population, Δn_{H1}, between the two spin states of the H1 subband have been compared. The total carrier density, n_{SdH}, has been employed in the calculations rather than the carrier density in only the H1 subband, n_{H1}, because the electric field $\langle E \rangle$ is, to a good approximation, proportional to n_{SdH}.

The calculated carrier densities in both the H1 and E2 subbands at various gate voltages agree with the experimental values for a well width, d_w, of 21 ± 2 nm. A simulation of the X-ray diffraction results in 22 ± 2 nm, in agreement with the above value. It should be emphasized that the occupation of the E2 subband depends mainly on the well width and not on the details of the self-consistently calculated Hartree potential. Furthermore the well width and hence the calculated carrier densities for two additional QWs, an asymmetric and a symmetric QW, have been corroborated by simulations of the corresponding X-ray diffraction results.

Finally Rashba spin–orbit splitting has also been observed and described quantitatively for a number of QWs in which only one conduction subband is occupied. No abnormal temperature and B dependence has been observed [38], ruling out magneto-intersubband scattering [39].

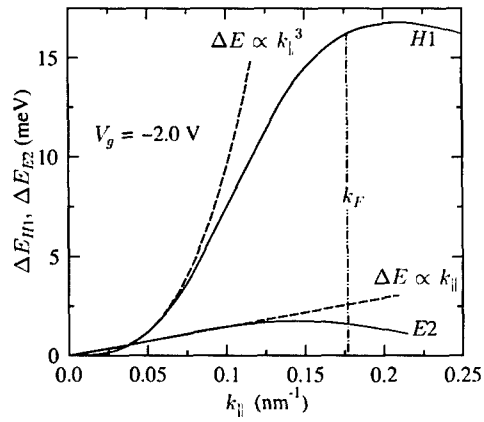

Fig. 7. The calculated spin splitting energy of the H1 and E2 subbands (solid curves), ΔE_{H1} and ΔE_{E2}, versus in-plane wave vector $k_{\|}$ for sample Q1605. The position of the Fermi wave vector k_F is denoted by the dotted-dashed line. The two dashed lines demonstrate the proportionality to $k_{\|}^3$ and $k_{\|}$, respectively, at small $k_{\|}$ values.

Winkler [37] has demonstrated that spin splitting for the heavy hole like state $|\Gamma_8, \pm 3/2\rangle$ should be proportional to $k_{\|}^3$ for small $k_{\|}$ values. The spin split heavy hole subband dispersion can be expressed as

$$E_{\pm}(k_{\|}) = \frac{h^2 k_{\|}^2}{2m^*} \pm \beta k_{\|}^3 \quad (4)$$

where β is the spin–orbit coupling constant between the Γ_8 and Γ_6 bands. In contrast, spin splitting for the electron like state $|\Gamma_6, \pm 1/2\rangle$ and the light hole like state $|\Gamma_8, \pm 1/2\rangle$, should be a linear function of $k_{\|}$. This is in good agreement with the self-consistently calculated ΔE_{H1} and ΔE_{E2} vs. $k_{\|}$ behavior shown in Fig. 7; the H1 conduction subband in a type III HgTe QW with an inverted band structure is principally a heavy hole state, and the E2 subband is an admixture of the light hole and electron state.

4.4. Magneto-transport; p type modulation doped QWs

Experimental results shown in Fig. 8 for a p type asymmetrically modulation doped QW, Q1441, with an inverted band structures display pronounced and complex SdH oscillations, which begin below 0.3T, and well developed quantum Hall plateaus. This QW also has a large mobility, i.e. $\mu = 1.0 \times 10^5$ cm^2 V^{-1} s^{-1}. If $d\rho_{xx}/dB$ is plotted vs. $1/B$, two periods can easily be distinguished, which are due to the indirect band gap. A Fast Fourier transformation (FFT) of the SdH oscillations for various hole concentrations in this gated p type QW results in two frequencies corresponding to the concentrations p_1 and p_2. The total hole concentration, p_2, is in good agreement with the Hall concentration at low magnetic fields. $p_2/p_1 = 4$, within experimental uncertainties, for $p_2 < 5 \times 10^{11}$ cm^{-2} [9]. p_2 can be increased up to 1.1×10^{12} cm^{-2}, however, above 5×10^{11} cm^{-2} the peak corresponding to p_1 disappears, in good agreement with theoretical calculations discussed below.

At hole concentrations of less than approximately 5×10^{11} cm^{-2} a contour plot of the intersection of the Fermi energy with that of the first valence subband, H2, results in four equivalent unconnected areas. For $p_2 > 5 \times 10^{11}$ cm^{-2} the Fermi contour resembles a single distorted ring [40]. The experimental results are in good agreement with the theoretical prediction of four equivalent valleys.

4.5. Magneto-transport; n type modulation doped QWs with Mn

QWs with Mn in the upper barrier with different spacer thickness between the HgTe and $Hg_{0.3}Cd_{0.68}Mn_{0.02}Te$ layers have different transport properties; when the spacer is reduced from 15 to 10 nm both the carrier concentration and mobility remain the same within experimental uncertainties or decrease slightly, however, a further reduction to 5 nm causes a significant reduction in these values.

As expected from their high mobilities, well developed SdH oscillations have been observed. Fourier analysis of these spectra reveal two spin split components of the H1 subband as well as the sum frequencies. The population difference between the two spin split components decreases with more positive gate voltages. This is caused by a reduction in the structure inversion asymmetry due to a larger electron concentration and hence a higher Fermi energy. The relative population difference $\Delta n_{H1}/n_{sym}$, where $n_{sym} = n_{H1}$ when $\Delta n_{H1} = 0$, is plotted in Fig. 9 vs. the normalized charge carrier concentration, $(n_{sym} - n_{H1}/n_{sym})$, in order to facilitate a suitable comparison of the QWs with spacer thicknesses of 5, 10 and 15 nm.

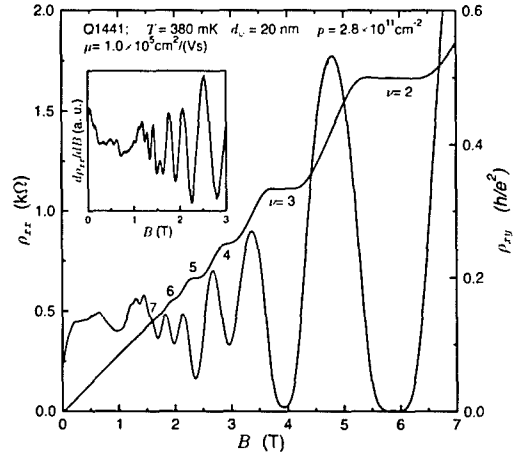

Fig. 8. ρ_{xx} and ρ_{xy} vs. B for a p type asymmetrically modulation doped QW with an inverted band structure at 380 mK. $d\rho_{xx}/dB$ is plotted vs. B in the inset.

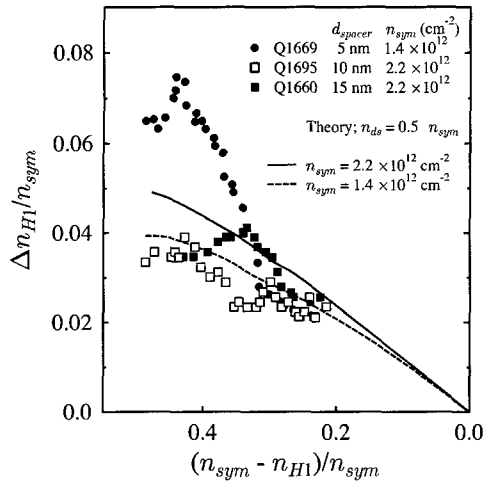

Fig. 9. The relative difference in population of the H1− and H1+ subbands as a function of normalized charge carrier concentration for QWs with spacer thicknesses of 5, 10 and 15 nm.

As can be seen in Fig. 9, theoretical calculations are in good agreement with experiment for the two QWs with thicker spacers. In contrast self-consistent Hartree calculations for the case of a 5 nm spacer, which do not take Mn into account, under estimate the experimental population difference by a factor of approximately 2.

If this enhanced population difference were due to *giant* Zeeman splitting, then it should be strongly temperature dependent [41] contrary to experimental results which show no change between 380 mK and 4.2 K. Therefore we infer that Mn increases the asymmetry of the QW structure and thus enhances Rashba spin–orbit splitting.

In addition to this desired influence of Mn, decreasing the spacer thickness reduces both the 2D electron concentration and the electron mobility. Nevertheless, electron mobilities of 0.6, 0.8 and 1.1×10^5 $cm^2\,V^{-1}\,s^{-1}$ have been achieved when Mn is separated from the well by 5, 10 and 15 nm thick spacers, respectively.

5. Conclusions

Selected aspects of MBE growth of $Hg_{1-x}Cd_xTe$ and $HgTe/Hg_{1-x}Cd_xTe$ heterostructures have been discussed.

By means of an optical investigation of $HgTe/Hg_{1-x}Cd_xTe$ SLs with a normal band structure combined with calculations based on an (8×8 **k·p**) model, it has been demonstrated that the energy separation between the H1–E1 and L1–E1 intersubband transition energies is primarily determined by the valence band offset, Λ, between HgTe and CdTe. This has led to unambiguous values for the offset and its temperature dependence, i.e. $\Lambda(T)=570\pm60$ meV and $d\Lambda/dT=-0.40$ meV/K. Furthermore the energy gap of HgTe at room temperature has also been determined to be −160 meV.

Magneto-transport studies have been performed on both n and p type modulation doped HgTe single QWs with inverted band structure. Rashba spin splitting in n type QWs with an inverted band structure has been investigated at different electron concentrations via a gate voltage. A large Rashba spin splitting has been observed, which is due to the heavy hole nature of the first conduction subband, H1. SdH oscillations of p type QWs display two periods, which have been shown to be due to their indirect band gap and the resulting multiple valleys, and not due to Rashba spin–orbit splitting. Both n and p modulation doped HgTe QWs, have high mobilities of up to 6×10^5 and 1.0×10^5 $cm^2\,V^{-1}\,s^{-1}$, respectively.

The results of magneto-transport experiments on HgTe QWs with Mn in the upper barrier are in good agreement with self-consistent Hartree calculations when the Mn is separated from the 2D electrons by spacers of 10 and 15 nm. However, the observed population difference of the two spin split states for a QW with a 5 nm spacer is larger than theoretical predictions by at least a factor of two. We conclude that Mn increases the asymmetry of the QW.

Acknowledgments

The support of the Deutsche Forschungsgemeinschaft via SFB 410, the Volkswagen Foundation (X.C. Zhang) and the Max Plank Gesellschaft (Y.S. Gui) is gratefully acknowledged.

References

[1] R.D. Rajaval, D.M. Jamba, J.E. Jensen, J.A. Wilson, J.L. Johnson, E.A. Patten, K. Kosai, P. Goetz, S.M. Johnson, J. Cryst. Growth 184/185 (1998) 1272.
[2] C.R. Becker, V. Latussek, A. Pfeuffer-Jeschke, G. Landwehr, L.W. Molenkamp, Phys. Rev. B 62 (2000) 10353.
[3] M. Dobrowolska, A. Mycielski, W. Dobrowolski, Solid State Commun. 27 (1978) 1233.
[4] V. Latussek, C.R. Becker, G. Landwehr, R. Bini, L. Ulivi, unpublished.
[5] Y. Kim, A. Ourmazd, M. Bode, R.D. Feldman, Phys. Rev. Lett. 63 (1989) 636.
[6] C.R. Becker, V. Latussek, W. Spahn, F. Goschenhofer, S. Oehling, G. Landwehr, in: R.E. Longshore, J.W. Baars (Eds.), Growth and Characterization of Materials for Infrared Detectors, SPIE Proc., vol. 2554, 1995, p. 6.
[7] Y.A. Bychkov, E.I. Rashba, J. Phys. C 17 (1984) 6039.
[8] X.C. Zhang, A. Pfeuffer-Jeschke, K. Ortner, V. Hock, H. Buhmann, C.R. Becker, G. Landwehr, Phys. Rev. B 63 (2001) 245305.
[9] K. Ortner, X.C. Zhang, A. Pfeuffer-Jeschke, C.R. Becker, G. Landwehr, L.W. Molenkamp, Phys. Rev. B, in press.
[10] F. Goschenhofer, J. Gerschütz, A. Pfeuffer-Jeschke, R. Hellmig, C.R. Becker, G. Landwehr, J. Electron. Mater. 27 (1998) 532.
[11] J.P. Laurenti, J. Camassel, A. Bouhemadou, B. Toulouse, R. Legros, A. Lusson, J. Appl. Phys. 67 (1990) 6454.
[12] M. Li, C.R. Becker, R. Gall, W. Faschinger, G. Landwehr, Appl. Phys. Lett. 71 (1997) 1822.

[13] M. Li, R. Gall, C.R. Becker, T. Gerhard, W. Faschinger, G. Landwehr, J. Appl. Phys. 82 (1997) 4860.
[14] D. Fasold, K. Heil, S. Jetschke, Phys. Stat. Sol. A 86 (1984) 125.
[15] L.R. Ram-Mohan, K.H. Yoo, R.L. Aggarwal, Phys. Rev. B 38 (1988) 6151.
[16] N.F. Johnson, H. Ehrenreich, P.M. Hui, P.M. Young, Phys. Rev. B 41 (1990) 3655.
[17] A. Simon, D. Bertho, D. Boiron, C. Jouanin, Phys. Rev. B 42 (1990) 5221.
[18] J.R. Meyer, C.A. Hoffman, F.J. Bartoli, Semicond. Sci. Technol. 5 (1990) S90.
[19] L. De Caro, L. Tapfer, Phys. Rev. B 51 (1995) 4374.
[20] M.H. Weiler, in: R. Willardson, A.C. Beer (Eds.), Semiconductors and Semimetals, 16, Academic Press, New York, 1981, p. 119.
[21] C.K. Shih, W.E. Spicer, Phys. Rev. Lett. 58 (1987) 2594.
[22] J. Schmidt, K. Ortner, J.E. Jensen, C.R. Becker, J. Appl. Phys. 91 (2002) 451.
[23] L. He, C.R. Becker, R.N. Bicknell-Tassius, S. Scholl, G. Landwehr, J. Appl. Phys. 73 (1993) 3305.
[24] K. Ortner, X.C. Zhang, S. Oehling, J. Gerschütz, A. Pfeuffer-Jeschke, V. Hock, C.R. Becker, G. Landwehr, L.W. Molenkamp, J. Appl. Phys. 79 (2001) 3980.
[25] M.A. Berding, A. Sher, J. Electron. Mater. 28 (1999) 799.
[26] S. Oehling, M. Ehinger, T. Gerhard, C.R. Becker, G. Landwehr, M. Schneider, D. Eich, H. Neureiter, R. Fink, M. Sokolowski, E. Umbach, Appl. Phys. Lett. 73 (1998) 3205.
[27] Z. Yang, Z. Yu, Y. Lansari, S. Hwang, J.W. Cook, J.F. Schetzina, Phys. Rev. B 49 (1994) 8096.
[28] C. Tanguy, Phys. Rev. Lett. 75 (1995) 4090, and references therein.
[29] K.A. Harris, R.W. Yanka, L.M. Mohnkern, A.R. Riesinger, T.H. Myers, Z. Yang, Z. Yu, S. Hwang, J.F. Schetzina, J. Vac. Sci. Technol. B 10 (1992) 1574.
[30] J.R. Meyer, A.R. Reisinger, K.A. Harris, R.W. Yanka, L.M. Mohnkern, L.R. Ram-Mohan, J. Cryst. Growth 138 (1994) 981.
[31] C.L. Cesar, M.N. Islam, R.D. Feldman, R.F. Austin, D.S. Chemla, L.C. West, A.E. DeGiovanni, Appl. Phys. Lett. 56 (1990) 283.
[32] G.L. Hansen, J.L. Schmit, T.N. Casselman, J. Appl. Phys. 53 (1982) 7099.
[33] M. von Truchsess, V. Latussek, C.R. Becker, E. Batke, J. Cryst. Growth 159 (1996) 1128.
[34] R. Sporken, S. Sivananthan, J.P. Faurie, D.H. Ehlers, J. Fraxedas, L. Ley, J.J. Pireaux, R. Caudano, J. Vac. Sci. Technol. A 7 (1989) 427.
[35] D. Eich, K. Ortner, U. Groh, Z.N. Chen, C.R. Becker, G. Landwehr, R. Fink, E. Umbach, Phys. Stat. Sol. A 173 (1999) 261.
[36] C.R. Becker, V. Latussek, M. Li, A. Pfeuffer-Jeschke, G. Landwehr, J. Electron. Mater. 28 (1999) 826.
[37] R. Winkler, Phys. Rev. B 62 (2000) 4245.
[38] X.C. Zhang, A. Pfeuffer-Jeschke, K. Ortner, C.R. Becker, G. Landwehr, Phys. Rev. B 65 (2002).
[39] T.H. Sander, S.N. Holmes, J.J. Harris, D.K. Maude, J.C. Portal, Phys. Rev. B 58 (1998) 13856.
[40] G. Landwehr, J. Gerschütz, S. Oehling, A. Pfeuffer-Jeschke, V. Latussek, C.R. Becker, Physica E 6 (2000) 713.
[41] D. Keller, D.R. Yakovlev, B. König, W. Ossau, Th. Gruber, A. Waag, L.W. Molenkamp, Phys. Rev. B 65 (2002).